NASA/TM—2010-216221 ISABE–2009–1189

Comparisons of Flutter Analyses for an Experimental Fan

Milind A. Bakhle
Glenn Research Center, Cleveland, Ohio

T.S.R. Reddy
The University of Toledo, Toledo, Ohio

George L. Stefko
Glenn Research Center, Cleveland, Ohio

April 2010

NASA STI Program . . . in Profile

Since its founding, NASA has been dedicated to the advancement of aeronautics and space science. The NASA Scientific and Technical Information (STI) program plays a key part in helping NASA maintain this important role.

The NASA STI Program operates under the auspices of the Agency Chief Information Officer. It collects, organizes, provides for archiving, and disseminates NASA's STI. The NASA STI program provides access to the NASA Aeronautics and Space Database and its public interface, the NASA Technical Reports Server, thus providing one of the largest collections of aeronautical and space science STI in the world. Results are published in both non-NASA channels and by NASA in the NASA STI Report Series, which includes the following report types:

- TECHNICAL PUBLICATION. Reports of completed research or a major significant phase of research that present the results of NASA programs and include extensive data or theoretical analysis. Includes compilations of significant scientific and technical data and information deemed to be of continuing reference value. NASA counterpart of peer-reviewed formal professional papers but has less stringent limitations on manuscript length and extent of graphic presentations.

- TECHNICAL MEMORANDUM. Scientific and technical findings that are preliminary or of specialized interest, e.g., quick release reports, working papers, and bibliographies that contain minimal annotation. Does not contain extensive analysis.

- CONTRACTOR REPORT. Scientific and technical findings by NASA-sponsored contractors and grantees.

- CONFERENCE PUBLICATION. Collected papers from scientific and technical conferences, symposia, seminars, or other meetings sponsored or cosponsored by NASA.

- SPECIAL PUBLICATION. Scientific, technical, or historical information from NASA programs, projects, and missions, often concerned with subjects having substantial public interest.

- TECHNICAL TRANSLATION. English-language translations of foreign scientific and technical material pertinent to NASA's mission.

Specialized services also include creating custom thesauri, building customized databases, organizing and publishing research results.

For more information about the NASA STI program, see the following:

- Access the NASA STI program home page at *http://www.sti.nasa.gov*

- E-mail your question via the Internet to *help@sti.nasa.gov*

- Fax your question to the NASA STI Help Desk at 443–757–5803

- Telephone the NASA STI Help Desk at 443–757–5802

- Write to:
  NASA Center for AeroSpace Information (CASI)
  7115 Standard Drive
  Hanover, MD 21076–1320

NASA/TM—2010-216221 ISABE–2009–1189

Comparisons of Flutter Analyses for an Experimental Fan

Milind A. Bakhle
Glenn Research Center, Cleveland, Ohio

T.S.R. Reddy
The University of Toledo, Toledo, Ohio

George L. Stefko
Glenn Research Center, Cleveland, Ohio

Prepared for the
19th International Society for Air Breathing Engines Conference (ISABE 2009)
sponsored by the International Society for Air Breathing Engines
Montreal, Quebec, Canada, September 7–11, 2009

National Aeronautics and
Space Administration

Glenn Research Center
Cleveland, Ohio 44135

April 2010

Acknowledgments

Support for this work from the NASA Fundamental Aeronautics Program is gratefully acknowledged. The authors would like to thank Dr. James Heidmann (Associate Principal Investigator for the Subsonic Fixed Wing Project) and Mr. Dale Hopkins (Associate Principal Investigator for the Supersonics Project) for their support of this work.

This work was sponsored by the Fundamental Aeronautics Program at the NASA Glenn Research Center.

Level of Review: This material has been technically reviewed by technical management.

Available from

NASA Center for Aerospace Information
7115 Standard Drive
Hanover, MD 21076–1320

National Technical Information Service
5301 Shawnee Road
Alexandria, VA 22312

Available electronically at http://gltrs.grc.nasa.gov

Comparisons of Flutter Analyses for an Experimental Fan

Milind A. Bakhle
National Aeronautics and Space Administration
Glenn Research Center
Cleveland, Ohio 44135

T.S.R. Reddy
The University of Toledo
Toledo, Ohio 43606

George L. Stefko
National Aeronautics and Space Administration
Glenn Research Center
Cleveland, Ohio 44135

Abstract

Two propulsion aeroelasticity codes were used to model the aeroelastic characteristics of an experimental forward-swept fan that encountered flutter during wind tunnel testing. Both of these three-dimensional codes model the unsteady flowfield due to blade vibrations using the Navier-Stokes equations. In the first approach, the unsteady flow equations are solved using an implicit time-marching approach. In the second approach, the unsteady flow equations are converted to a harmonic balance form and solved using a pseudo-time marching method. This paper describes the flutter calculations and compares the results to experimental measurements.

Introduction

Aircraft engine turbomachinery blades are susceptible to aeroelastic vibration problems and high-cycle fatigue failures. Flutter stability is likely to become a major challenge as aggressive new designs of fan, compressor and turbine blades are developed to reduce noise, improve performance, and reduce weight. Hence, it is important to develop and validate numerical tools that can be used to verify aeroelastic stability using high-fidelity physics-based models. Such numerical tools will enable gas turbine designers to develop new turbomachinery blading that will not flutter, thus improving safety, reducing development cycle time and cost, and enabling the targeted improvements listed earlier.

Research has been on-going in the development, validation and application of high-fidelity models for aeroelastic vibrations in aircraft engine fan, compressor, and turbine blades (Ref. 1). Recent work has included time-domain solution of the Reynolds-averaged Navier-Stokes (RANS) equations to provide the unsteady flowfield and unsteady aerodynamic forces on the blades. An example of such work is the TURBO aeroelastic analysis code (Refs. 2 and 3). Such high-fidelity time-domain models require large numbers of computations and a long time for startup transients to decay before the final periodic solution is obtained. A second approach is to use the periodicity in time of typical turbomachinery flows to represent each flow variable by a Fourier series in time, leading to a harmonic balance form of the Navier-Stokes equations (Ref. 4). Solutions to these equations can be obtained using methods that are typically used for steady flow problems such as pseudo-time marching and local time stepping. Thus, the harmonic balance approach leads to a method that can be significantly faster than the typical time-domain solution method (Ref. 4).

In the present study, the configuration selected is an experimental fan (Ref. 5) for which wind-tunnel measurements of performance and flutter vibrations are available. This fan was designed with aggressive goals for performance and noise reduction. During wind-tunnel testing, the fan performed well at design speed, and was successfully throttled to the stall line. However, flutter was encountered just above the operating line at part-speed conditions. The flutter mode was identified as the first bending mode of the airfoil, in a two nodal diameter forward-traveling wave pattern. In this paper, a comparison is presented between two flutter analyses applied to this fan: a time-domain RANS aeroelastic code (Ref. 2) (TURBO) and a harmonic balance (HB) RANS aeroelastic analysis and computer code developed by Hall et al. (Refs. 4 and 6). Both analyses solve the three-dimensional unsteady, Reynolds-Averaged Navier-Stokes equations with the ability to model a rotating blade row with harmonic blade vibrations or incoming periodic distortions. For flutter calculations, the blade vibration is prescribed to be the modal deflection and a frequency, both of which are calculated from a separate structural dynamics analysis. Computations are performed in a single blade passage for both steady and unsteady analyses. In the time-domain analysis (Ref. 2), the unsteady pressures are used to calculate a work-per-cycle that is then used to calculate the aerodynamic damping, which is used to determine aeroelastic stability in the selected vibration mode and traveling wave pattern. In the harmonic balance analysis, the resulting unsteady pressures are used to calculate a generalized aerodynamic force and then an eigenvalue problem is solved to calculate the aerodynamic

damping, which is used to determine stability of the blade in a specific vibration mode (Ref. 7).

Note that both the aeroelastic codes were run with small amplitude vibrations of the fan blade to calculate linearized unsteady aerodynamics for a conventional linear flutter analysis. However, both the analysis procedures can also be used for larger amplitudes of vibration.

Analysis

Aeroelastic Model

The equations of motion for a fan blade (with all blades assumed to be identical) can be written as

$$[M]\{\ddot{q}\}+[K]\{q\}=[A]\{q\} \tag{1}$$

where $[M]$ and $[K]$ are generalized mass and stiffness matrices, $\{q\}$ is the generalized displacement vector, and $[A]$ is the blade vibration-dependent generalized aerodynamic force matrix. The matrices $[M]$, $[K]$, and $[A]$ are of size $NM \times NM$; $\{q\}$ is of size $NM \times 1$; NM is the number of modes.

The elements of $[M]$ and $[K]$ are obtained from a free-vibration analysis using a commercial structural dynamics analysis software. The matrices $[M]$ and $[K]$ are diagonal and their non-zero elements are related as

$$K_i = M_i \omega_i^2 (1 + 2i\zeta) \tag{2}$$

where ω_i is the natural frequency of the i^{th} mode, and ζ is the structural damping ratio; usually the mode shapes are mass-normalized and therefore $M_i = 1$.

Since all the blades are identical (that is, a tuned rotor), the aeroelastic modes consist of individual blades vibrating with equal amplitudes at a fixed interblade phase angle between adjacent blades. Hence, the motion of the s^{th} blade in r^{th} interblade phase angle mode can be written as

$$\{q_s\} = \{q_r\} e^{i\omega t}\, e^{i\sigma_r s} \tag{3}$$

where ω is the vibration frequency, σ_r is the interblade phase angle related to nodal diameter (ND) pattern of the traveling wave and number of blades N_{blades} as

$$\sigma_r = 2\pi\, ND / N_{\text{blades}} \tag{4}$$

Thus, the equations of motion for a blade become

$$-\omega^2[M]\{q_r\}+[K]\{q_r\}=[A_r]\{q_r\} \tag{5}$$

The following subsections describe the flutter calculation method used with the harmonic balance code and separately with the time-domain TURBO code.

HB Flutter Analysis

The HB flutter analysis requires calculation of elements of the generalized aerodynamic force matrix $[A_r]$. Unsteady flowfield computations are carried out for each vibration mode and assumed frequency. For a selected value of interblade phase angle, the harmonic balance code is used to calculate the unsteady pressure distribution on the blade surface, which is further used to calculate the (complex-valued) elements of the generalized aerodynamic force matrix $[A_r]$. This calculation is repeated for N_{blades} interblade phase angles given by Equation (4).

To calculate flutter stability, Equation (5) is written in a standard eigenvalue form as:

$$[[P]-\gamma[Q]]\{q_r\}=\{0\} \tag{6}$$

where

$[P]=([K]-[A_r])/\omega_o^2$; $[Q]=[M]$; $\gamma = (\omega/\omega_o)^2$ and ω_o is the assumed frequency used in the calculation of the elements of the aerodynamic force matrix $[A_r]$.

The solution of the above eigenvalue problem results in NM complex eigenvalues of the form

$$i(\omega/\omega_o)=i\sqrt{\gamma}=\bar{\mu}\pm i\bar{\nu} \tag{7}$$

The real part of the eigenvalue ($\bar{\mu}$) represents the damping ratio, and the imaginary part ($\bar{\nu}$) represents the damped frequency; flutter occurs if $\bar{\mu} \geq 0$ for any eigenvalue.

In the present work, structural damping is set to zero and therefore damping is referred to as aerodynamic damping. Also, note that $\bar{\mu}$ is opposite in sign to damping.

TURBO Work-Per-Cycle Method

The work-per-cycle approach is used to determine flutter stability. First, the flowfield through the blade row is calculated with no prescribed blade vibration. Starting with this converged steady flowfield, blade vibrations are prescribed in a selected mode, frequency, and nodal diameter pattern or phase angle. After the transients in the flowfield decay, and a periodic flowfield is obtained, the work done on the vibrating blade is calculated for a cycle of blade vibration as follows:

$$W = \oint \int_{\text{surface}} -p\,dA \cdot (\partial X / \partial t)\,dt \tag{8}$$

where, p is the blade surface pressure and A is the surface area vector. For harmonic vibration, the work-per-cycle of oscillation, can be rewritten as

$$W = \oint \int_{\text{surface}} -pdA \cdot \delta q_0 \omega \cos(\omega t) dt \tag{9}$$

The aerodynamic damping ratio (ζ) associated with blade vibration is related to the work-per-cycle (W) and the average kinetic energy (K_E) of the blade over one cycle of vibration through the following equation (Ref. 8)

$$\frac{W}{K_E} = -\frac{8\pi\zeta}{\sqrt{1-\zeta^2}} \tag{10}$$

where

$$K_E = \frac{1}{T}\oint \frac{1}{2} m V^2 dt \tag{11}$$

$$\zeta = C/C_{cr} \; ; \quad C_{cr} = 2m\omega \tag{12}$$

In the preceding equations, C is the damping, C_{cr} is the critical damping, m is the mass of the blade, V is the surface velocity due to blade vibration, and T is the time period.

For small values of damping ratio which typically occur in aeroelastic calculations of interest, $\zeta << 1$, the aerodynamic damping ratio can be approximated as

$$\zeta \approx -W/8\pi K_E \tag{13}$$

If aerodynamic damping is negative, flutter can occur. Note that the structural damping (material and mechanical damping) has not been considered. Also, note that aerodynamic damping (ζ) is opposite in sign to $\overline{\mu}$.

Results

In this section, the results of the steady and unsteady computations are presented. Steady and unsteady computations were carried out at rotational speeds of 100 percent (design), 85, and 75 percent. The part-speeds were selected to correspond to the speeds at which large vibratory responses due to flutter were encountered on the stall side of the operating line during testing. No flutter was encountered during testing at 100 percent speed.

Note that in the present work, the harmonic balance aeroelastic code was run with very small amplitude vibrations of the fan blade to calculate linearized unsteady aerodynamics for a conventional linear flutter analysis. Also, the amplitude of vibration for the time-domain computations was in a linear range.

Steady Computational Results

In this study, the airfoil geometry used was calculated based on static deflections obtained from structural analysis for 85 percent speed. The static deflections included the effects of rotational speed, applied pressures, and blade temperatures; nonlinear geometry effects were also included in the analyses. The blade geometry at 85 percent speed and nominal operating conditions was used for all computations. Previous calculations (Ref. 2) for this case have shown that changes from the nominal blade geometry due to changes in rotational speed were not significant and therefore a single geometry was used for computations at all speeds and operating conditions in the present work. The computational grid used was generated using commercial software. The grid for the harmonic balance computations is shown in Figure 1(a); the grid size is 193×33×49 for the O-grid block that wraps around the blade airfoil with 193 grid points around the airfoil, 33 grid points in the circumferential direction, and 49 grid points in the spanwise direction. The H-grid blocks in the inlet and exit sections are each 17×33×49 with 17 points in the streamwise direction, 33 grid points in the circumferential direction, and 49 grid points in the spanwise direction. The tip clearance was based on rig test measurements and is modeled using 9 points between the blade tip and casing. For the TURBO time-domain computations, the H-grid, shown in Figure 1(b), has a size of 121×51×39; 4 cells are used in the tip clearance region.

The inlet flow conditions used in the computations consisted of circumferentially-averaged radial profiles of total pressure, total temperature, and flow angles. These prescribed profiles were based on rig measurements, supplemented by previous steady computations. The exit flow conditions consisted of a circumferentially-averaged radial profile of static pressure. This profile, which was based on pressure measurements at design speed, was used with uniform scaling for the computations at all speeds and at all conditions.

Steady computations were carried out for three fixed rotational speeds (100, 85, and 75 percent). For each speed, the exit pressure profile was uniformly scaled to vary the mass flow rate and the operating point on the fan map. Thus, three speedlines were generated using each analysis code. Figure 2 shows the convergence of the steady harmonic balance computations as a plot of non-dimensional torque with iteration counter (100 iterations per counter). The computations were carried out at 85 percent speed for various values of imposed backpressure at the exit boundary. As can be noted from Figure 2, excellent convergence was obtained for all operating conditions. Similar convergence was obtained for the computations at the other speeds as well as for the computations with the TURBO code at all speeds. All steady results presented here are from well-converged solutions.

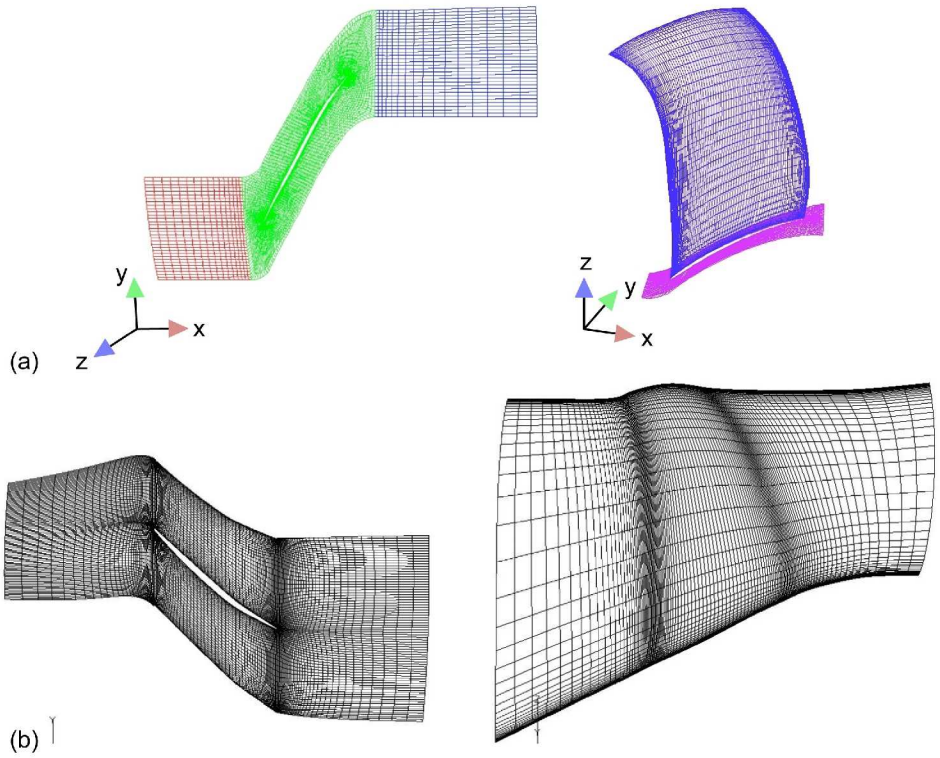

Figure 1.—(a) Computational mesh for harmonic balance (HB) computations.
(b) Computational mesh for time-domain TURBO computations.

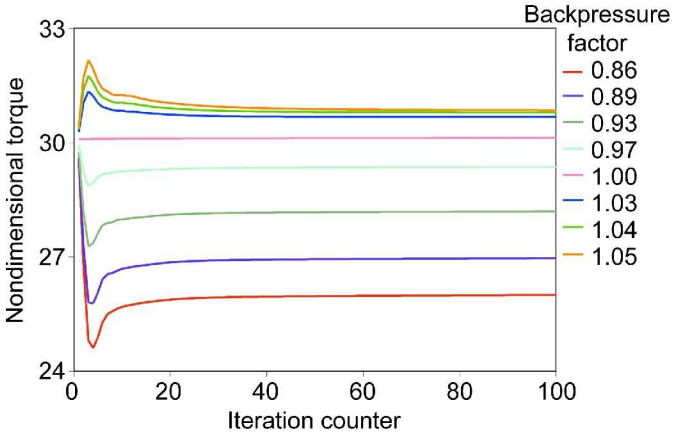

Figure 2.—Steady solution convergence (HB).

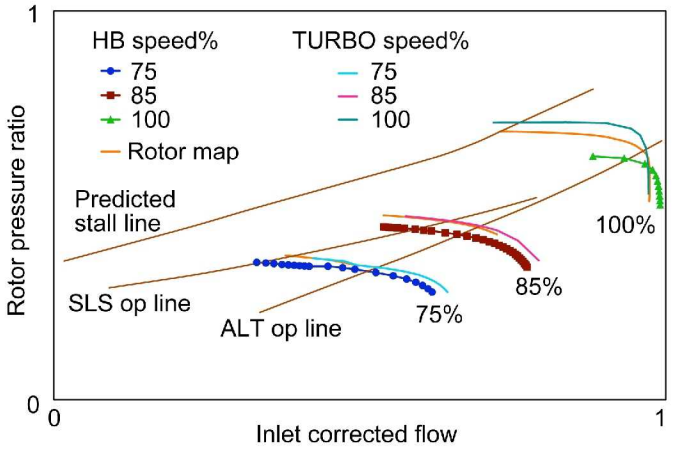

Figure 3.—Nondimensionalized fan map showing performance predictions from harmonic balance and TURBO codes.

The fan map is shown in Figure 3 with the results of harmonic balance steady computations denoted as HB and the results of the TURBO computations. Several computations were done for 75, 85, and 100 percent speeds. All computed results correlate well with measurements. Of particular interest is the last condition computed on the stall side, beyond which no converged solutions were obtained. For the HB results, the predicted pressure ratio is approximately 3 percent lower at 75 and 85 percent speeds, and approximately 4.5 percent lower at 100 percent speed. For the TURBO results, the predicted pressure ratio is approximately 1.5 percent higher at 100 percent speed and nearly identical at the other two speeds. For the HB results, the mass flow rate at the near-stall point is lower than measurements at 75 percent speed, in excellent agreement at the 85 percent speed, and significantly higher at the 100 percent speed. For the TURBO results, the mass flow rate is higher at the part speeds, and nearly the same at 100 percent speed. Note that the stall line shown in Figure 3 was estimated based on prior experience and was not confirmed during rig testing because of the occurrence of

flutter. Also, since the stall side was of primary interest, no attempt was made to determine the upper bound on choke flow.

Overall, the HB results show good correlation with the TURBO results, except for a slight shift in the speed lines towards lower mass flow rate and lower pressure ratio for both 75 and 85 percent speeds. At 100 percent speed, the HB results are shifted towards lower pressure ratio, and slightly higher mass flow rate. At 75 and 85 percent speeds, the HB calculations provide converged results for lower mass flow rates than were obtained with TURBO. Also, the HB results consistently show a slightly lower pressure ratio as compared to TURBO and the test data. These differences need to be investigated further. It should be noted that significant differences exist between the numerical method used in the TURBO computations and the HB computations. These differences include time-domain versus frequency-domain, numerical discretization, grid, and algorithm used to solve the RANS equations, turbulence modeling, and others. Therefore, the differences in results noted in Figure 3 are not entirely surprising.

To examine the sensitivity of the HB computed results to numerical parameters, the second and fourth order smoothing parameters, which are necessary to ensure numerical stability, were varied, respectively, between 0.25 and 1, and between 0.002 and 0.006, as listed in Table 1. The results shown in Figure 4 indicate that no significant change in pressure ratio resulted from the stated variation in these numerical parameters. The mass flow variation was less than 0.5 percent.

TABLE 1.—RANGE OF NUMERICAL SMOOTHING PARAMETERS USED TO STUDY VARIABILITY OF HB COMPUTED PERFORMANCE

Case	Smoothing parameter	
	2nd order	4th order
1	1.0 (nominal)	0.006 (nominal)
2	1.0	0.002 to 0.005
3	0.25	0.002

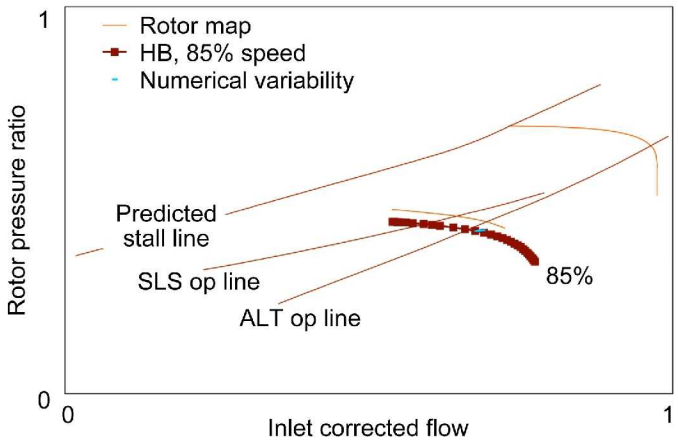

Figure 4.—Nondimensionalized fan map showing variability in results due to numerical smoothing parameters.

Unsteady Computational Results

Vibration Mode 1

Unsteady computations were performed using the harmonic balance code at 100, 85, and 75 percent speeds to predict the aeroelastic stability of the blade. The first blade vibration mode and several nodal diameters covering the entire possible range were considered. Various steady conditions were considered from near peak-efficiency to near the stall line. This allowed the trend along the speed line to be assessed. Note that the results presented in this paper were all computed with only the 0th and 1st harmonics included in the aerodynamic analysis using the harmonic balance method.

Figure 5 shows the convergence of the unsteady computations as a plot of non-dimensional generalized force (real and imaginary parts) with iteration counter (100 iterations per counter) for various nodal diameters. These computations were for 85 percent speed and for an operating point near the peak-efficiency condition with a non-dimensional backpressure of 1.0. As can be noted, although the rates of convergence vary with nodal diameter, all the results are well-converged. Similar convergence characteristics were observed at the near-stall condition with a nondimensional backpressure value of 1.05.

A sensitivity study was performed to investigate the effect of the unsteady grid scaling parameter. The nominal value of this numerical input parameter was increased by factors of 2 and 5, and then decreased by the same factors. There was no change in the generalized force results within plotting accuracy – demonstrating that for the present calculations, the prescribed unsteady grid scaling has no effect on the results. Recall that in the present study, the harmonic balance aeroelastic code was run with very small amplitude vibrations of the fan blade to calculate linearized unsteady aerodynamics for a conventional linear flutter analysis.

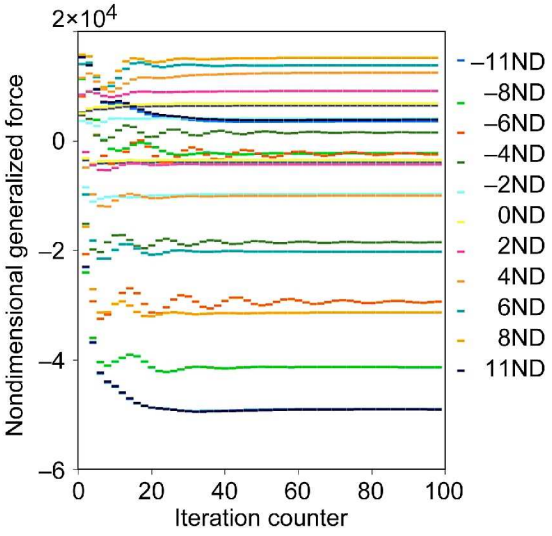

Figure 5.—HB unsteady solution convergence.

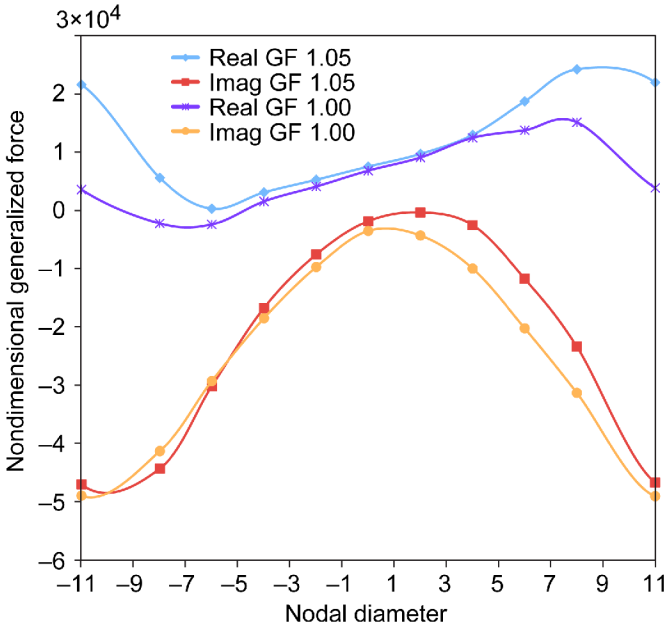

Figure 6.—HB generalized force variation with nodal diameter.

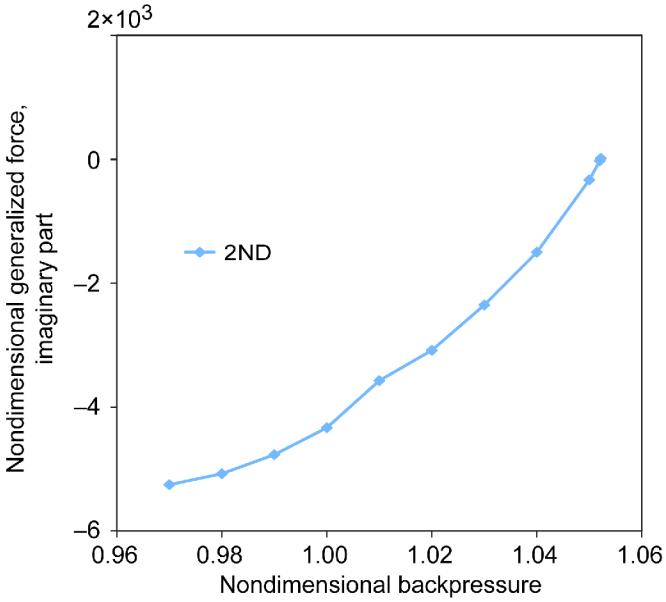

Figure 7.—Variation of HB generalized force (imaginary part) with backpressure for *ND* = 2.

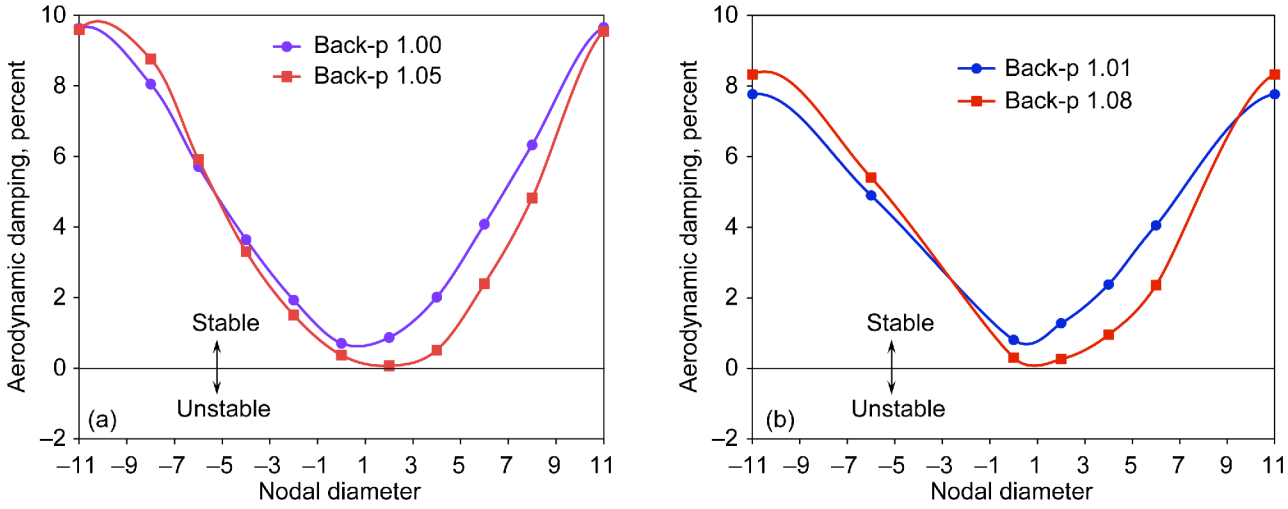

Figure 8.—(a) Variation of HB aerodynamic damping with nodal diameter at 85 percent speed. (b) Variation of TURBO aerodynamic damping with nodal diameter at 85 percent speed.

Figure 6 shows the variation of the converged generalized force with nodal diameter for the two different values of backpressure at 85 percent speed. For a single vibration mode, the stability is determined by the imaginary part of the generalized force and Figure 6 shows that the stability varies significantly with nodal diameter. Further, with the change in backpressure from peak-efficiency towards stall, it can be seen that the imaginary part of the generalized force drops closer to zero at *ND* = 2. This trend is seen more clearly in Figure 7. The imaginary part of the generalized force is seen to clearly move towards zero as the backpressure increases – going from peak-efficiency towards stall. Note that Figure 7 includes results at nondimensional backpressure values of 1.052 and 1.0522, with a change in the sign of the imaginary part occurring between these conditions.

The generalized force was used to calculate the aerodynamic damping, which is plotted in Figure 8(a). The results are presented for backpressure values near peak-efficiency (1.0) and near-stall (1.05) conditions. The aerodynamic damping is seen to vary by an order of magnitude with nodal diameter of the traveling wave, with the minimum occurring at *ND* = 2 (forward traveling wave). Note that although the damping value is nearly zero at the near-stall condition, it is still positive even at its minimum value, indicating stability at a nondimensional backpressure of 1.05.

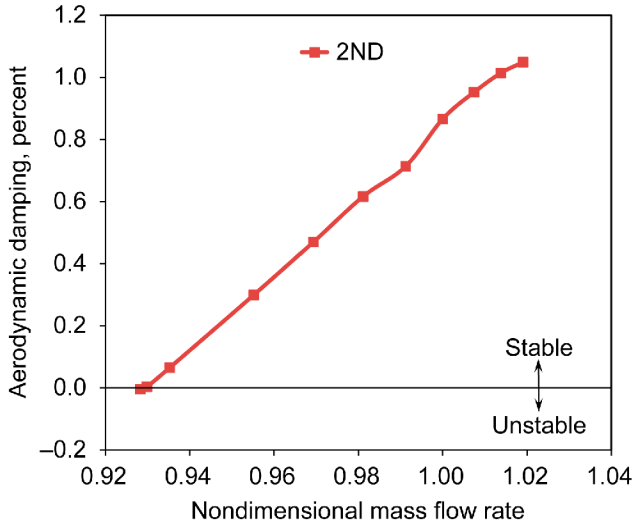

Figure 9.—Variation of HB aerodynamic damping with nondimensional mass flow rate for *ND* = 2 at 85 percent speed.

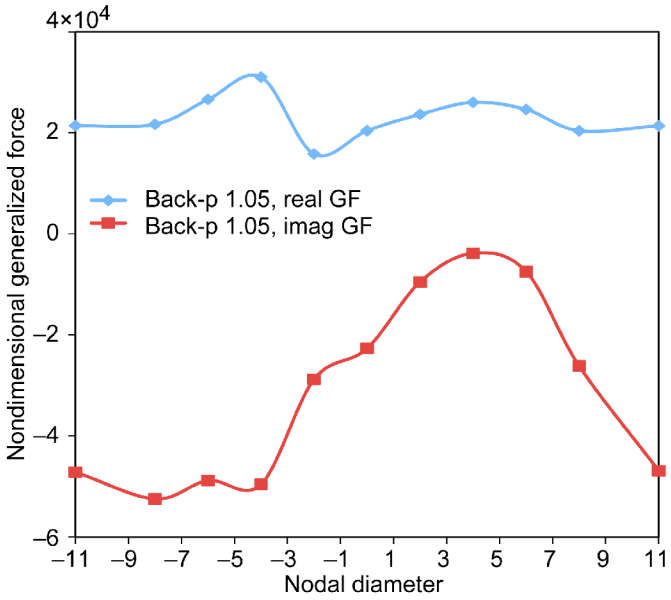

Figure 10.—HB generalized force variation with nodal diameter for mode 2 at 85 percent speed.

The aerodynamic damping calculated from the TURBO code is shown in Figure 8(b) as a variation with nodal diameter. Note that the backpressure values are slightly different for the TURBO results and the HB results. Also, the TURBO computations were done for fewer nodal diameter than with the HB code. A comparison of the results in Figure 8(a) and (b) clearly shows that both methods predict very similar variations with nodal diameter. Further the variation in damping values is nearly the same, as are the trends going from peak efficiency to near stall operating conditions (increasing backpressure).

Additional calculations were carried out for a small increase in backpressure to identify the condition of zero aerodynamic damping (flutter). In the absence of these additional results at backpressure of 1.052 and 1.0522, it would be necessary to extrapolate the damping as a function of mass flow to identify the flutter point. Figure 9 shows the variation of aerodynamic damping with mass flow rate with a clear monotonic drop in stability along the speed line towards stall.

For the TURBO computations, the aerodynamic damping was linearly extrapolated to obtain the flutter condition since the last computed condition near stall showed a small positive aerodynamic damping.

Vibration Mode 2

To verify that the mode 1 is the most unstable mode, HB unsteady computations were carried out for mode 2 at 85 percent speed. The generalized force variation with nodal diameter, shown in Figure 10, is somewhat similar to that for mode 1 shown in Figure 6. Note that *ND* = 4 is the least damped nodal diameter. Unsteady computations were carried out for *ND* = 4 and 2 for various steady operating conditions

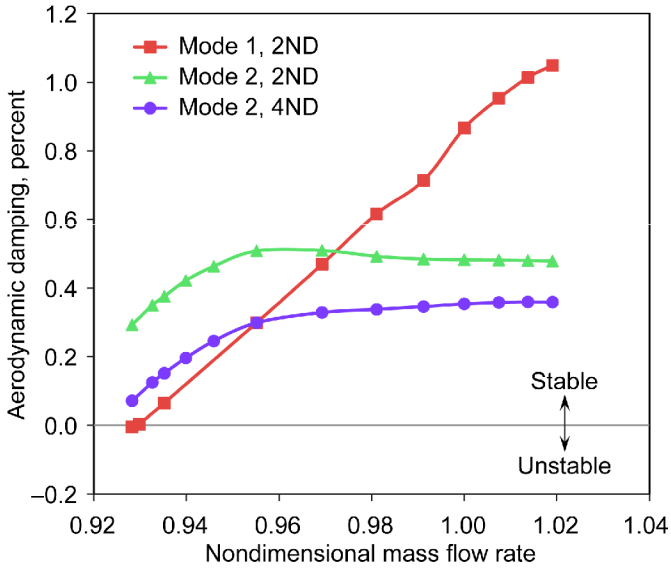

Figure 11.—Variation of HB aerodynamic damping with nondimensional mass flow rate for modes 1 and 2 at 85 percent speed.

(backpressure values or mass flow rate values). Figure 11 shows that mode 1 2ND is the most unstable and mode 2 4ND has a very slightly higher damping. The rate of decrease of damping with decreasing mass flow rate is very similar for both modes as the stall line is approached.

Other Rotational Speeds

The results of unsteady calculations at 75 percent speed show trends that are nearly the same as those in Figures 5 to 9. Figure 12 shows the corresponding variation of aerodynamic

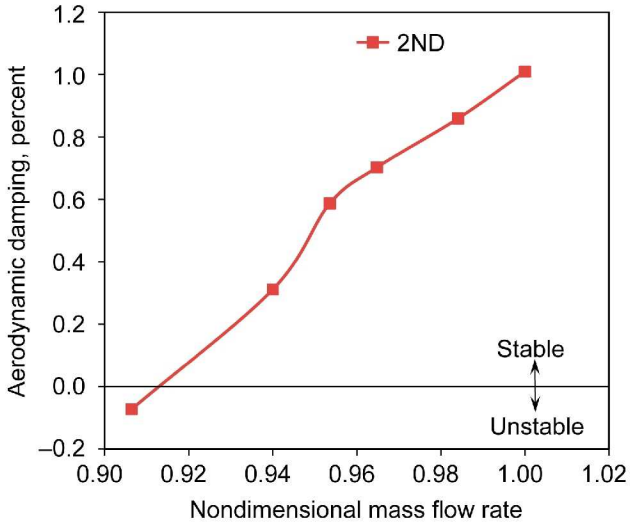

Figure 12.—Variation of aerodynamic damping with nondimensional mass flow rate for mode 1 *ND* = 2 at 75 percent speed.

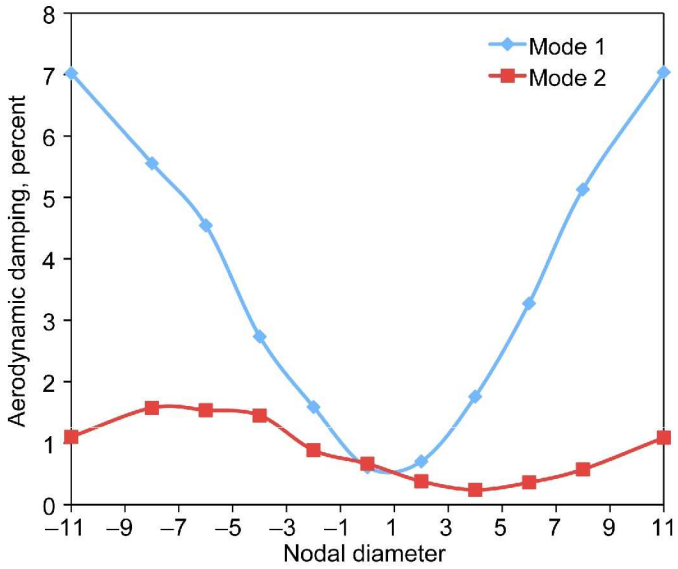

Figure 13.—Variation of aerodynamic damping with nodal diameter for modes 1 and 2 at 100 percent speed.

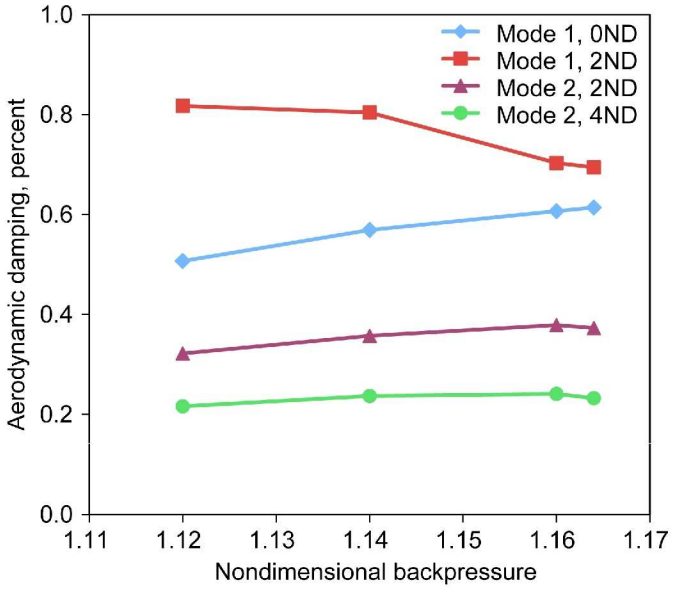

Figure 14.—Variation of aerodynamic damping with backpressure for modes 1 and 2 at 100 percent speed.

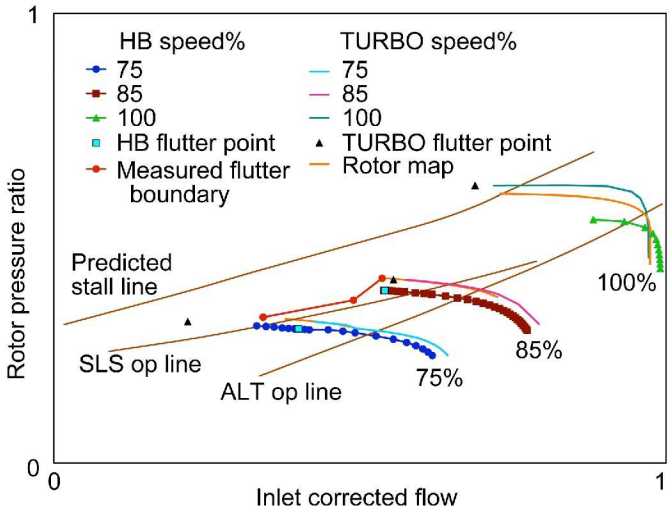

Figure 15.—Fan map showing calculated flutter point along with the measured flutter boundary.

damping along the 75 percent speed line. Note that the aerodynamic damping is clearly negative at the lowest mass flow rate condition and the flutter point is obtained by interpolation.

The results of unsteady calculations at 100 percent speed for modes 1 and 2 are shown in Figures 13 and 14. The variations with nodal diameter are somewhat similar to the those for 85 percent speed. However, the variations with backpressure (mass flow rate) show a very small slope in contrast to those seen in Figures 11 and 12. Based on the calculated aerodynamic damping and its small variation with backpressure, it is inferred that no flutter will occur at 100 percent speed.

The calculated flutter points at 85 and 75 percent speeds are plotted on the fan map along with the measured flutter boundary in Figure 15. It can be seen that the calculated flutter point is very close to the measured value at 85 percent sped with a difference of less than 0.5 percent in mass flow rate. As noted previously, the pressure ratio is slightly under-predicted and the difference from the measured data is 3 percent at the flutter point. For comparison, the flutter point calculated using TURBO is also plotted. Both calculations are very close to the test data; the present calculated result is slightly closer to the measurement in mass flow rate, but farther in pressure ratio as compared to the TURBO result.

At 75 percent speed, the difference between the present results and measurements is higher (about 4 percent) than at 85 percent speed. The TURBO result also shows a larger difference from measurement at 75 percent speed than at 85 percent speed.

At 100 percent speed, no flutter point is predicted by the HB analysis and the flutter point predicted by TURBO is beyond the stall line, meaning that the operating condition will not be reached.

Conclusions

Steady and unsteady computations have been carried out using two Propulsion Aeroelasticity codes. These aeroelastic analysis codes solve the Reynolds-Averaged Navier-Stokes equations with blade vibrations using a time-marching method (TURBO) and a harmonic balance method (HB). The configuration selected was an experimental fan that encountered flutter during wind tunnel testing. The computational results were summarized and compared with experimental data. Overall, both TURBO and HB results are in good agreement with experimental data. The steady results were compared on the performance map and showed good correlation with data. However, the steady HB results under-predict the pressure ratio slightly and the steady TURBO results are closer to the measurements. Also, the HB analysis provides solutions at slightly lower mass flow rates than were obtained with TURBO at part-speed conditions. The HB results under-predict the pressure ratio by about 3%. A detailed look at the flowfields predicted by HB and TURBO may provide additional information regarding the source of the differences. A numerical study with the smoothing parameters in the HB analysis showed that the calculated performance is not sensitive to these numerical parameters.

The flutter results from both HB and TURBO correlated very well with the experimental data. The least stable vibration mode matched experimental observations. The least stable nodal diameter pattern (interblade phase angle) also matched correctly with the experimental observations. The calculated flutter conditions agreed closely with the experimental data. A sensitivity study on the grid motion scaling parameter showed that the computational results were insensitive to variations in the selected value of this parameter, thus demonstrating the linearity of the results for the selected small amplitude of blade vibration.

Computations for the first two vibration modes showed that the first mode had a slightly lower aerodynamic damping, correctly correlating with the experimental observations. Computations at three rotational speeds (100, 85, and 75 percent) showed that flutter would be encountered at the part-speed conditions but not at the design condition, matching the experimental observations.

In the present study, very small amplitude vibrations were prescribed to calculate linearized unsteady aerodynamics for a conventional linear flutter analysis as a first step to understand the characteristics of the harmonic balance code and of the flutter of an experimental fan. Future work will investigate the non-linear amplitude-dependent effects using the same harmonic balance aeroelastic code and the time-domain TURBO code.

References

1. Marshall, J.G., and M. Imregun, "A review of aeroelasticity methods with emphasis on turbomachinery applications," *Journal of Fluids and Structures*, vol. 10, 1996, pp. 237–267.
2. Bakhle, M.A., Srivastava, R., Panovsky, J., Keith, T.G., Jr., Stefko, G.L., "Flutter Calculations of an Experimental Fan," Paper US-2, CEAS/AIAA/NVvL International Forum on Aeroelasticity and Structural Dynamics, Amsterdam, June 4–6 2003.
3. Srivastava, R., Bakhle, M.A., and Keith, T.G., Jr., "Numerical Simulation of Aerodynamic Damping for Flutter Analysis of Turbomachinery Blade Rows," *Journal of Propulsion and Power*, vol. 19, no. 2, March–April 2003.
4. Hall, K.C., Thomas, J.P., and Clark, W.S., "Computation of Unsteady Nonlinear Flows in Cascades Using a Harmonic Balance Technique," *AIAA Journal*, vol. 40, no. 5, May 2002.
5. Weir, D., "NASA AST – AOI 14, Design and Test of Fan and Nacelle Models for Quiet High Speed Fan – Final Report," NASA/CR—2003-212370, July 2003.
6. Ekici, K., Hall, K.C., "Nonlinear Analysis of Unsteady Flows in Multistage Turbomachines Using Harmonic Balance," *AIAA Journal*, vol. 45, no. 5, May 2007, pp. 1047–1057.
7. Bakhle, M.A., Thomas, J.P., and Reddy, T.S.R., "Fan Flutter Computations Using the Harmonic Balance Method," AIAA Paper 2008–4743, July 2008.
8. Carta, F.O., "Coupled Blade-Disk-Shroud Flutter Instabilities in Turbojet Engine Rotors," *Journal of Engineering for Power*, July 1967, pp. 419–426.

REPORT DOCUMENTATION PAGE			Form Approved OMB No. 0704-0188

1. REPORT DATE *(DD-MM-YYYY)*	2. REPORT TYPE	3. DATES COVERED *(From - To)*
01-04-2010	Technical Memorandum	

4. TITLE AND SUBTITLE
Comparisons of Flutter Analyses for an Experimental Fan

5a. CONTRACT NUMBER

5b. GRANT NUMBER

5c. PROGRAM ELEMENT NUMBER

6. AUTHOR(S)
Bakhle, Milind, A.; Reddy, T.S.R.; Stefko, George, L.

5d. PROJECT NUMBER

5e. TASK NUMBER

5f. WORK UNIT NUMBER
WBS 561581.02.08.03.21.03

7. PERFORMING ORGANIZATION NAME(S) AND ADDRESS(ES)
National Aeronautics and Space Administration
John H. Glenn Research Center at Lewis Field
Cleveland, Ohio 44135-3191

8. PERFORMING ORGANIZATION REPORT NUMBER
E-17202

9. SPONSORING/MONITORING AGENCY NAME(S) AND ADDRESS(ES)
National Aeronautics and Space Administration
Washington, DC 20546-0001

10. SPONSORING/MONITOR'S ACRONYM(S)
NASA

11. SPONSORING/MONITORING REPORT NUMBER
NASA/TM-2010-216221

12. DISTRIBUTION/AVAILABILITY STATEMENT
Unclassified-Unlimited
Subject Categories: 07 and 05
Available electronically at http://gltrs.grc.nasa.gov
This publication is available from the NASA Center for AeroSpace Information, 443-757-5802

13. SUPPLEMENTARY NOTES

14. ABSTRACT
Two propulsion aeroelasticity codes were used to model the aeroelastic characteristics of an experimental forward-swept fan that encountered flutter during wind tunnel testing. Both of these three-dimensional codes model the unsteady flowfield due to blade vibrations using the Navier-Stokes equations. In the first approach, the unsteady flow equations are solved using an implicit time-marching approach. In the second approach, the unsteady flow equations are converted to a harmonic balance form and solved using a pseudo-time marching method. This paper describes the flutter calculations and compares the results to experimental measurements.

15. SUBJECT TERMS
Fan blades; Flutter; Navier-Stokes equation; Turbomachinery; Aeroelasticity

16. SECURITY CLASSIFICATION OF:			17. LIMITATION OF ABSTRACT	18. NUMBER OF PAGES	19a. NAME OF RESPONSIBLE PERSON
a. REPORT	b. ABSTRACT	c. THIS PAGE			STI Help Desk (email:help@sti.nasa.gov)
U	U	U	UU	15	19b. TELEPHONE NUMBER *(include area code)* 443-757-5802